J. Ocean Eng. Mar. Energy (2015) 1:395–404
DOI 10.1007/s40722-015-0028-0

RESEARCH ARTICLE

The "Wave Bridge" for bypassing oceanic wave momentum

Sebastian Timmerberg[1] · **Thomas Börner**[1] · **Mostafa Shakeri**[1] · **Reza Ghorbani**[2] · **Mohammad-Reza Alam**[1]

Received: 1 October 2014 / Accepted: 4 May 2015 / Published online: 4 June 2015

Abstract Here, we introduce and investigate the concept of the Wave Bridge that can bypass the momentum of oceanic waves about ocean objects. The Wave Bridge is composed of a wave energy absorber on the upstream side of an ocean object, and a wave maker on its downstream side. The wave absorber and the wave maker are mechanically connected in such a way that the wave energy absorbed on the upstream side is simultaneously used by the wave maker downstream of the ocean object to generate waves. The Wave Bridge therefore protects the ocean object from waves by transferring incident wave energy from the upstream to the downstream. Furthermore, since the wave absorbed upstream is the same as the one generated downstream, the corresponding horizontal forces are equal in magnitude and opposite in sign and hence cancel each other, resulting in a zero net horizontal force on the Wave Bridge and its supporting structure. Our experimental results show a wave protection efficiency of up to 97 % and a horizontal force protection efficiency of up to 80 %. We also investigate the effect of the finite height of the Wave Bridge and the resulting wave energy leakage underneath the plungers on the overall protection efficiency. The Wave Bridge and its variants may reduce the costs of offshore structures by reducing the wave loads, provide calm water in the midst of an energetic ocean for future offshore cities, and conserve energy of dynamic position systems by reducing the wave-induced disturbances of vessels.

Keywords Experimental hydrodynamics · Wave load protection · Offshore structures · High-efficiency wave energy absorption · Wave maker

✉ Mohammad-Reza Alam
reza.alam@berkeley.edu

Sebastian Timmerberg
sebastian.timmerberg@googlemail.com

Thomas Börner
thomas.boerner@rwth-aachen.de

Mostafa Shakeri
shakeri@berkeley.edu

Reza Ghorbani
rezag@hawaii.edu

[1] Department of Mechanical Engineering, University of California, Berkeley, CA 94720, USA

[2] Department of Mechanical Engineering, University of Hawaii at Manoa, Honolulu, HI 96822, USA

1 Introduction

Oceanic waves carry both energy and momentum. A wave energy harvester placed upstream of an ocean object can absorb the incident wave energy, but not the horizontal momentum. As a result while waves disappear downstream of the harvester, the wave force is to be endured by the structure that the wave harvester is attached to. The higher the efficiency of the wave energy absorption, the lesser are waves downstream, however, higher horizontal net force are thus induced into the structure. Now, consider a wave maker installed downstream of the structure generating exactly the same amount of energy absorbed upstream by the harvester. The wave maker exerts a horizontal force on the supporting structure, but in the opposite direction of the force of the wave absorber. If the wave maker and wave absorber have the same shape and configuration, then the magnitude of the two horizontal forces, theoretically, must be exactly the same. If furthermore the wave absorber and the wave maker have correct relative phase, then the sum of the horizontal forces will be zero. Here, we present the Wave Bridge, a mechanical device consisting of two plungers which are directly connected to each other to create a protected area

with calm water in between the wave maker and the wave absorber. This is the main idea behind the Wave Bridge (cf. Fig. 1). The entire Wave Bridge including both plungers and their mechanical connection is hinged onto an ocean object. Since in the ideal case the net horizontal force on the hinged point is zero and the stress induced by wave forces only occurs in the mechanical connection, the Wave Bridge shields the ocean object from wave impact. In other words, waves are forced to bypass the ocean structure through the Wave Bridge, just as momentum bypasses intermediate spheres in the Newton's cradle resulting in a zero net force on bypassed spheres.

Specifically in our Wave Bridge design, we use wedge-shaped plunger-type wave energy harvester and wave maker that, if properly made for a specific ocean environment, can theoretically have an efficiency of unity (i.e., absorb the entire energy of incoming waves). In this case, the entire wave energy and wave momentum can be bypassed about the ocean structure. Thus, the protected ocean structure does not experience any waves or any wave-induced horizontal forces. A plunger-type wedge-shaped wave maker (and an equal wave absorber) is an asymmetric two-dimensional wedge-shaped float with one vertical side and one sloped side. As this plunger moves in the vertical direction, it generates waves on the sloped side, while not much waves will be excited on the flat side. These devices are typically surface piercing and their vertical extent may or may not reach the bottom. In this sense, they are almost the opposite of surge-type converters that are hinged at the bottom and, depending on their designs, may or may not reach the free surface.

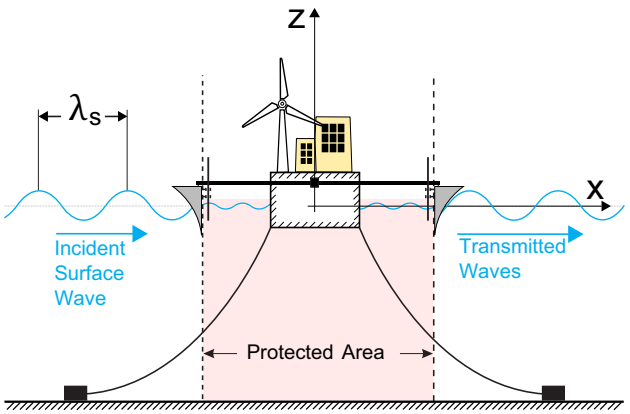

Fig. 1 Two-dimensional schematic presentation of the Wave Bridge. A wedge-shaped plunger absorbs incident wave energy upstream of the offshore structure and via a purely mechanical mechanism transfers it to the downstream of the structure by another wedge-shaped plunger that acts as a wave maker. As a result, waves bypass the offshore structure: the offshore structure does not experience wave action and the net horizontal force on the entire system is significantly reduced. The Wave Bridge may be connected to the offshore structure as shown or be independently supported. Note that since the net horizontal force on the Wave Bridge is small (ideally zero), only a small force is endured by the supporting structure

Plunger-type wedge-shaped wave makers and wave energy converters have been subjects of extensive studies since decades ago. A finite depth wedge in an infinite depth water was studied analytically and experimentally by Wang (1974). For the case of a finite depth water and for a wedge that has a flat vertical side on one side and a sloped surface on the other, Wu (1988) investigated the radiated waves to the right numerically using a boundary collocation method (BCM), where the no-flow boundary condition on the flat side of the plunger is assumed to extend to the seabed. For the case of a finite height plunger Wu (1991) used a boundary element method to determine radiated waves on both sides of the plunger. These numerical results agree well with our investigations (Ellix and Arumugam 1984; Patel and Ionnaou 1980; Henderson et al. 2006). Plunger-type wedge-shaped floaters have also been proposed for energy extraction (e.g. Hager et al. 2012; Count 1980; Evans 1976; Madhi et al. 2014) and as a break water (Hales 1981; He et al. 2012; Dong et al. 2008).

In this paper, we experimentally investigated both the wave protection efficiency and the horizontal momentum bypassing the efficiency of the Wave Bridge in a two-dimensional case with monochromatic, linear waves. We show via wave tank tests that a wave protection efficiency of up to 97 % and a horizontal force bypassing efficiency of up to 80 % can be obtained. Both maximum efficiencies are obtained when the frequency of the incident wave is close to the natural frequency of the Wave Bridge, but the bandwidth of acceptable perforation is relatively broad. If the Wave Bridge is deployed in deep water, the plungers will not extend to the seabed. Hence, wave energy will partly leak underneath the plungers in the protected zone resulting in waves in the protection zone. Numerical investigation, based on the boundary collocation method, are performed to address the leakage issue and therefore help to determine the theoretical efficiency of the Wave Bridge to create a protected zone.

Incident wave force, particularly its horizontal component, clearly increases the structural costs of offshore structures. The presented Wave Bridge provides a simple design to significantly reduce such forces on offshore structures. This is more highlighted in areas with poor foundation and in deep waters. Wave Bridge may also help conserving energy of dynamic positioning system by reducing the wave-induced motion of a vessel. The efficiency and economic advantages of the Wave Bridge idea is more pronounced if a single Wave Bridge is deployed about a group of offshore structures, say, about an offshore wind farm. Wave Bridge is a broadband wave protection mechanism that can theoretically be used both in shallow and deep waters.

2 Experimental details

2.1 Wave tank and wave maker

The experiments on the Wave Bridge were carried out in a wave tank at the University of California, Berkeley, that is 30 m long, 0.45 m wide, and 2.4 m deep. Transparent, 3 cm-thick glass panels are supported by steel frames and allow direct wave observation and optical measurements. Linear waves with frequencies below 0.9 Hz were generated with a paddle-type wave maker and higher frequency waves up to 1.75 Hz were generated by a plunger-type wave maker. The wave maker was located at one of the far ends of the wave tank. To minimize wave reflection, an artificial beach was placed at the opposite end of the tank. A schematic diagram of the experimental setup, including the wave tank, the plunger-type wave maker and the Wave Bridge is shown in Fig. 2. The paddle-type wave maker consists of a 0.45 m-wide and 1.9 m-high board that is hinged to the bottom of the wave tank. A crank connects the top of the board to the shaft of a motor. The crank pin on the motor side is connected to the motor shaft via a threaded rod, allowing for adjustment of the stroke of the board motion. The wave maker frequency is set by a control system. The plunger-type wave maker, however, consists of a wedge-shaped plunger made from marine plywood. It is driven by a voltage-controlled DC motor and is capable of generating waves up to a frequency of 1.75 Hz. The back side of the plunger is a 0.45 m-wide vertical board and the front side makes a 15° angle with the vertical plane. The wave maker can be submerged up to 45 cm, while the rotation of the motor shaft is converted into the linear motion of the plunger by a crank mechanism facilitating a stroke of up to 18 cm. Linear bearings are used to ensure a vertical motion of the wedge.

2.2 Wave Bridge

To evaluate the Wave Bridge concept, a two-dimensional model was designed and manufactured. The prototype (Fig. 4) consists of a mechanical system for transferring wave energy, a main frame (a) that includes bearings (e), a hinge and two identical wave-absorbing and wave-generating plungers (c). A schematic diagram of the Wave Bridge and close-up pictures of the fabricated prototype are shown in Figs. 3 and 4.

The role of the mechanical system of the Wave Bridge is to transfer momentum from the wave-absorbing plunger to the wave-making plunger. This system was designed to have minimal friction and moving parts. A 165 cm-long aluminum bar (2.5 cm wide × 3.8 cm high) connects the two plungers,

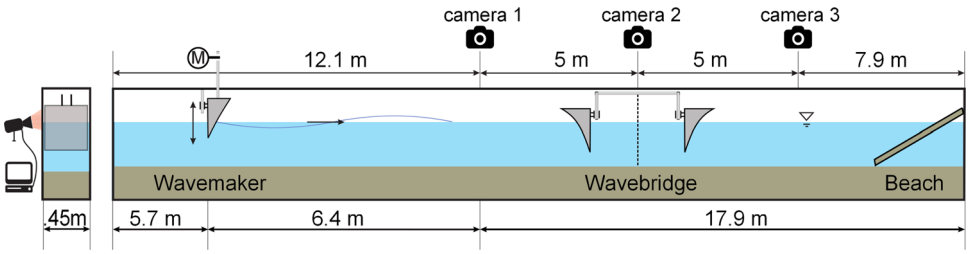

Fig. 2 Schematic side and end view diagrams of the experimental setup. A plunger-type wave maker generates a monochromatic wave of frequency up to 1.75 Hz, while an artificial beach minimizes wave reflection at the opposite end of the wave tank. The Wave Bridge is installed 11.4 m away from the wave maker into the tank. Three digital cameras are used to measure the wave parameters precisely.

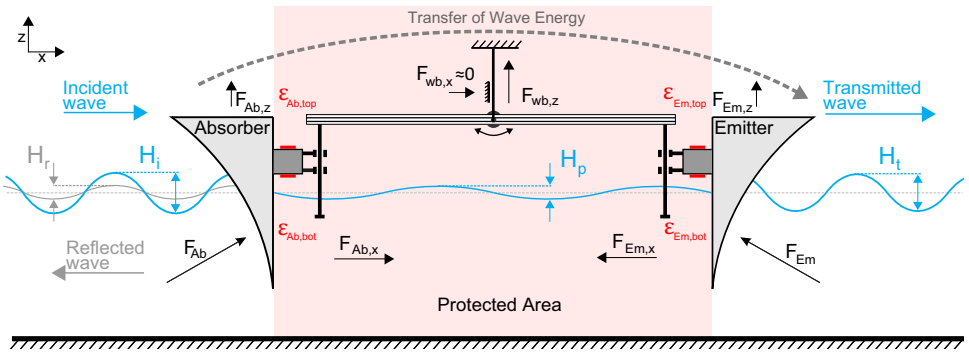

Fig. 3 Schematic diagram of the Wave Bridge along with the notations for the forces and wave parameters. Horizontal forces due to the interaction of waves with the Wave Bridge plungers have similar magnitudes but opposite signs, resulting in a vanishing net horizontal force on the entire structure. The *red stripes* represent the locations of strain gauge half-bridges, used for force measurements (color figure online)

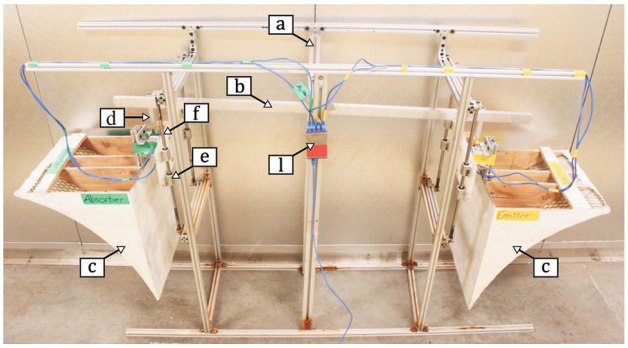

Fig. 4 The two-dimensional prototype of the Wave Bridge. The wave-absorbing plunger (*left*) is mechanically connected via a hinged aluminum bar to the wave-emitting plunger (*right*). Both the relatively lightweight plungers are made of fiberglass sheets and plywood, providing sufficient stiffness. Linear block bearings, guided on aluminum rods, restrict the plungers to a vertical motion. To accurately measure the force, strain gauge half-bridges were glued on the connection profiles between the plunger and the bearings (see Fig. 5 for details)

as seen in Fig. 4b. This bar is hinged to the main frame (a) at its longitudinal center to allow the upward and downward motion of the plungers (c). Each end of the aluminum bar has a 3.2 cm-wide and 20 cm-long flute to accommodate a guide for a 1 cm-wide wheel (2.8 cm in diameter). The shaft of each wheel is connected to a second, vertical aluminum bar (d) that is attached to the plunger as Fig. 5 shows. The main frame of the Wave Bridge system supports the linear bearings (e) that restrict the plungers' motion in the vertical direction.

The main frame of the Wave Bridge supports the forces from the bearings and the hinge and keeps the structure in position. Standard T-slotted aluminum profiles were used to build the main frame. The main frame occupies a space of 1.22 m × 1.25 m × 0.45 m, which fits into the wave tank. Four linear, closed bearings (e) with a dynamic load capacity of 1 kN are used to guarantee low friction. They are guided on two 1.27 cm rods (f) and align each plunger. The distance between the vertical sides of the plungers is set to 1.36 m.

The plungers are the main components of the Wave Bridge. Hager et al. (2012) studied the effects of the plunger geometry on the absorption efficiency. They showed that concave-shaped plungers yield the highest absorption of up to 94.5 % of the incident wave energy, but details of the plunger shape were not presented in their work. In the current investigation, we use a concave plunger whose shape is based on the distribution of the horizontal velocity component of a progressive wave. Both plungers are designed to match the size of the wave tank, resulting in maximum dimensions of the plungers as 45 cm × 45 cm × 55 cm (x-, y- and z-direction).

$$x(z) = 0.1122 \times \cos h(-3.241 \times (z + 0.717)) - 0.1292 \tag{2.1}$$

The plungers consist of a supporting framework made from four wooden panels (g) with a shape of Eq. (2.1) in meters that are mounted on a 3.175 mm-thick, 55 cm-high and 44 cm-wide piece of plywood, which acts as the vertical back side (h). The framework is covered by a mesh and resin-coated fiberglass (i), providing an optimal way to achieve a lightweight, sealed plunger with sufficient stiffness. The plungers are approximately 45 cm wide and 55 cm deep.

2.3 Wave measurement

Wave absorption and generation characteristics are the key factors in determining the overall performance of the Wave Bridge. The main part of the incident wave energy is absorbed, reflected, or dissipated. The remaining wave energy leaks underneath the plunger, thus reaching the protected region at the center of the Wave Bridge. To evaluate the performance of the Wave Bridge, transmission, absorption, and reflection of the incident wave are taken into account and the energy-based efficiencies are calculated. The total energy of a linear wave E per unit length is

$$E = E_\mathrm{p} + E_\mathrm{k} = \frac{\rho g H^2}{8} = \mathrm{const.} H^2, \tag{2.2}$$

where ρ is the water density in kg/m^3, g is the gravitational acceleration in m/s^2, and H is the wave height in m. The wave energy does not depend on the wave frequency or the wavelength. Thus, the efficiency for wave transmission η_t, reflection η_r, and protection η_p, are defined as

$$\eta_\mathrm{t} = \left(\frac{H_\mathrm{t}}{H_\mathrm{i}}\right)^2 \quad \eta_\mathrm{r} = \left(\frac{H_\mathrm{r}}{H_\mathrm{i}}\right)^2 \quad \eta_\mathrm{p} = \left(\frac{H_\mathrm{i} - H_\mathrm{p}}{H_\mathrm{i}}\right)^2, \tag{2.3}$$

where H_i is the incident wave height, H_r is the reflected wave height, and H_p is the wave height measured in the protected area between the two plungers.

The wave surface height was obtained using an optical measurement system. Images of the waves are recorded at 30 frames per second at three locations along the wave tank. Camera 1, which is placed 5 m upstream from the center of the Wave Bridge, records the incident and reflected waves, while camera 3 records the transmitted wave 5 m downstream, as shown in Fig. 2. The wave parameters between the absorbing and emitting plungers are recorded by camera 2, mounted at the center. All cameras were mounted outside the wave tank, recording the waves through the transparent wave tank panels from a horizontal distance of 40 and 20 cm below mean water level. Snell's law shows that the wave heights recorded by the cameras are underestimated by about 6.5 % for all of the waves measured in the current study. Yet, by evaluating the Wave Bridge's performance using wave height ratios, the error due to refraction in the wave tank glass cancels out in the

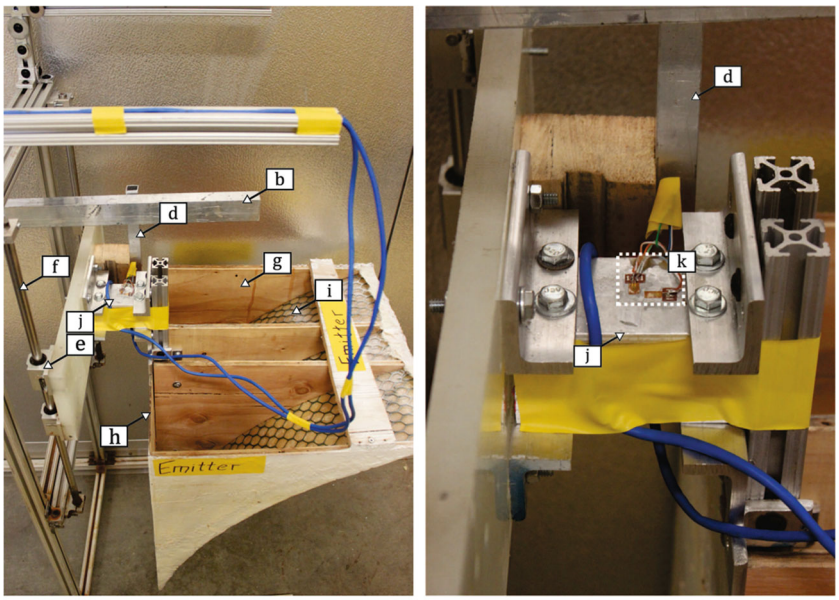

(a) (b)

Fig. 5 The emitter side of the Wave Bridge holding the plunger with a concave shape based on the vertical distribution of the horizontal velocity component of a progressive wave. Four linear pillow block bearings (*e*) on each side of the Wave Bridge restrict the plungers to a solely vertical motion. The plungers are connected through a hollow aluminum profile (*j*) to the linear bearings. Two half-bridges (*k*), each consisting of two strain gauges, are mounted on the *top* and *bottom side* of the connection for horizontal force measurements

current results. The cameras have a resolution of 1080 pixels × 1920 pixels. Each camera covers a view of approximately 70 cm by 40 cm. Additional light sources, shining from below into the wave tank, were used to increase the contrast at the water surface. To transform the wave height from the pixel domain to the physical domain in the laboratory coordinate system, a calibration grid of four black dots with known vertical and horizontal distance is attached to the transparent side panels of the wave tank. The vertical and horizontal numbers of pixels between the dots are related to the physical distances. Each pixel correlates to an area of 0.41 mm × 0.41 mm. Each frame of the videos is processed in MATLAB. The Canny edge detection technique (MathWorks, Inc., Boston, MA, USA) was used to extract the history of the free surface profiles. A method, developed by Goda and Suzuki (1976), based on trigonometric considerations, is then used to obtain the incident and reflected wave heights H_i and H_r from cameras 1 and 3. The wave within the Wave Bridge (camera 2) is not fully formed, since the distance between the plungers is in the range of the wavelength and the method by Goda and Suzuki leads to significant errors. Therefore, conservative approximation is used and the wave height H_p is determined as the maximum wave height measured within the Wave Bridge.

2.4 Force measurement

Horizontal forces due to absorption are counteracted by the forces of the wave-generating plunger and hence minimal horizontal net forces are expected to act on the system if a high wave transmission is achieved. However, reflection of the waves causes a horizontal force on the plunger and thus the supporting structure must provide the necessary counterforce. To minimize the horizontal net forces on the structure, the wave transmission must be maximized. To measure the resulting horizontal forces, four strain half-bridges, built from two active, 120 Ω resistance strain gauges with a gauge factor of $k = 2.03$ were used. For each side of the Wave Bridge, one of these half-bridges was glued onto the top side (*k*) and one on the bottom side of the hollow aluminum profile (*j*) connecting the plungers to the linear bearings. Figure 5b shows the basic pattern of one half-bridge used on one side of the aluminum profile making the half-bridge sensitive to both axial and bending strain. While one of the strain gauges of a half-bridge is mounted in the direction of axial/horizontal strain, the second gauge acts as a Poisson gauge and is mounted perpendicular to the principal axis of the strain.

The ratio of bridge-voltage to excitation voltage $\frac{U_{\mathrm{strain},i}}{U_0}$ of each of the half-bridges is measured using a data acquisition system shown in Fig. 4l. The *Catman Easy* software was used to read the data at a frequency of 200 Hz. Using the gauge factor k and the Poisson's ratio of $\nu_\mathrm{Alu} = 0.34$ for aluminum, the strain ϵ_i of each half-bridge $i \in$ (Em, top; Em, bot; Ab, top; Ab, bot) was calculated by

$$\epsilon_i = \frac{U_{\mathrm{strain},i}}{U_0} \frac{4}{(1+\nu_\mathrm{Alu})k}. \tag{2.4}$$

Thus, the horizontal and vertical forces of the absorber ($F_{\mathrm{Ab},x}$ and $F_{\mathrm{Ab},z}$) and the emitter ($F_{\mathrm{Em},x}$ and $F_{\mathrm{Em},z}$) are

$$\begin{aligned} F_{x,i} &= \frac{E_\mathrm{Alu}\, A}{2} (\epsilon_{i,\mathrm{top}} + \epsilon_{i,\mathrm{bot}}) \\ F_{z,i} &= \frac{E_\mathrm{Alu}\, W_x\, L}{2} (\epsilon_{i,\mathrm{top}} - \epsilon_{i,\mathrm{bot}}), \end{aligned} \tag{2.5}$$

with $E_{\mathrm{Alu}} = 70\ \frac{\mathrm{kN}}{\mathrm{mm}^2}$ and $A = 291\ \mathrm{mm}^2$ as the cross-sectional area of the hollow aluminum profile. Note that the vertical forces are induced through a momentum and thus have to be calculated using the section modulus W_x of the hollow aluminum profile as $W_x = \frac{B\,H^3 - b\,h^3}{6\,H} = 4568\ \mathrm{mm}^3$ with H, B, h and b as the outer and inner dimensions of the hollow aluminum profile.

Finally, the net horizontal and vertical forces are calculated as

$$F_{\mathrm{wb},x} = F_{\mathrm{Ab},x} - F_{\mathrm{Em},x} \quad F_{\mathrm{wb},z} = F_{\mathrm{Em},z} + F_{\mathrm{Ab},z}. \tag{2.6}$$

The efficiency of the horizontal force reduction η_{F} due to the protecting effect of the Wave Bridge is further defined as

$$\eta_{\mathrm{F}} = \frac{\mathrm{RMS}(F_{\mathrm{wb,stiff}}(t)) - \mathrm{RMS}(F_{\mathrm{wb},x}(t))}{\mathrm{RMS}(F_{\mathrm{wb,stiff}}(t))}. \tag{2.7}$$

Here, $F_{\mathrm{wb,stiff}}$ represents the initial forces of the incident wave impinging on the absorbing plunger, while suppressing any movements of the plungers. $F_{\mathrm{wb},x}$ is the horizontal net force for an operating Wave Bridge system. To shift the time resolved force signals to a single value for efficiency calculation, the root mean-squared (RMS) values of the signals were used. All RMS values are calculated for a minimum period of 20 s, while the Wave Bridge operates in a steady state. Experiments with the smallest wave loads lead to RMS values of $3.1 \times 10^{-3}\ \frac{\mathrm{mV}}{\mathrm{V}}$. Measurements under no load show an RMS noise value of $1.52 \times 10^{-4}\ \frac{\mathrm{mV}}{\mathrm{V}}$, yielding a maximum noise-to-signal ratio of 4.93 % and a signal-to-noise ratio of SNR = 13.09 dB, respectively.

3 Results and discussion

Two types of tests were conducted to experimentally assess the performance of the Wave Bridge. One test included the assessment of the Wave Bridge for a variable frequency ratio of the incident wave frequency to the natural frequency of the Wave Bridge (ω/ω_0), while the wave steepness ka was kept in the range of $0.09 < ka < 0.13$. For the other test series, the frequency ratio was kept constant, while ka of incident waves was varied. For all experiments, a plunger-type wave maker was placed about 17.1 m from the center of the Wave Bridge inside the wave tank with a mean water depth of 0.7 m. Cameras 1 and 3 recorded the surface elevation of the incident, reflected and transmitted waves, while camera 2 recorded the waves between the plungers, which were 48 cm submerged. Although a wave-absorbing beach was used at the end of the wave tank, the limited length of the tank led to wave reflection. Thus, the measurements were stopped when the waves reflected from the back wall returned to the wave-emitting side of the Wave Bridge.

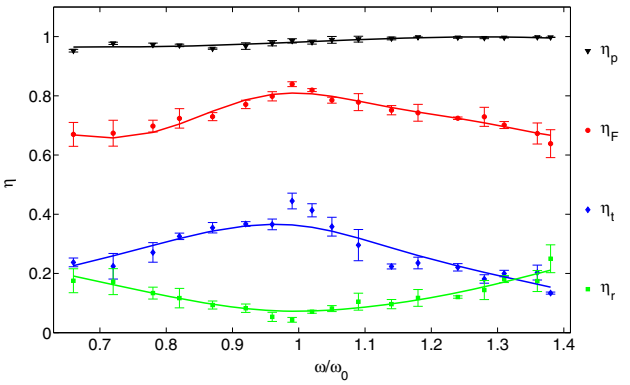

Fig. 6 Wave protection, transmission, reflection and horizontal force reduction efficiencies of the Wave Bridge as a function of the ratio of incident wave frequency, ω, to the Wave Bridge natural frequency, ω_0. The highest momentum transmission and net force reduction performances of the Wave Bridge are achieved at a ratio of 1, representing the resonance state and the smallest wave reflection at the absorbing plunger. The wave steepness, ka, was kept in the range of $0.09 < ka < 0.13$

Transmission, reflection, wave protection and the horizontal force reduction efficiencies (respectively η_{t}, η_{r}, η_{p} and η_{F}) are shown in Fig. 6 as a function of the ratio of the incident wave frequency to the natural frequency of the Wave Bridge (ω/ω_0). The incident wave frequency was varied between 0.83 and 1.75 Hz and the Wave Bridge used in our experiment has a natural frequency of 1.27 Hz for given water depth h. This leads to a frequency ratio range of 0.66–1.38 for all of the cases tested throughout the current study. To assess the influence of the incident wave frequency on the Wave Bridge performance, the steepness of the incident wave was kept in the range of $0.09 < ka < 0.13$, ensuring linear waves. Each of the averaged measurement points in Fig. 6 includes three actual measurement results.

The transmission efficiency is the highest ($\eta_{\mathrm{t}} \sim 40\,\%$) at the frequency ratio of unity where the reflection is the minimum ($\eta_{\mathrm{r}} \sim 5\,\%$), indicating that most of the wave energy has been transferred to the downstream side (Fig. 6). With very little pile-up of wave energy between the two plungers ($\eta_{\mathrm{p}} \sim 97\,\%$), we can conclude that the rest of the power is wasted by the dampings in the wave itself, friction between the incident wave and the sides of the tanks, friction between the incident wave and the Wave Bridge, and internal (mechanical) losses of the Wave Bridge. The transmission coefficient reduces and the reflection coefficient increases as we move away from the resonance, indicating more reflection and less transmission. The horizontal force reduction efficiency also gains a maximum at the resonance point ($\eta_{\mathrm{F}} \sim 80\,\%$) and decreases away from the resonance as expected. This can be explained by a less adaptive dynamic response of the Wave Bridge to the induced motion of the incident waves. As a consequence, a larger part of the incident wave energy is reflected from the absorbing plunger, resulting in a higher

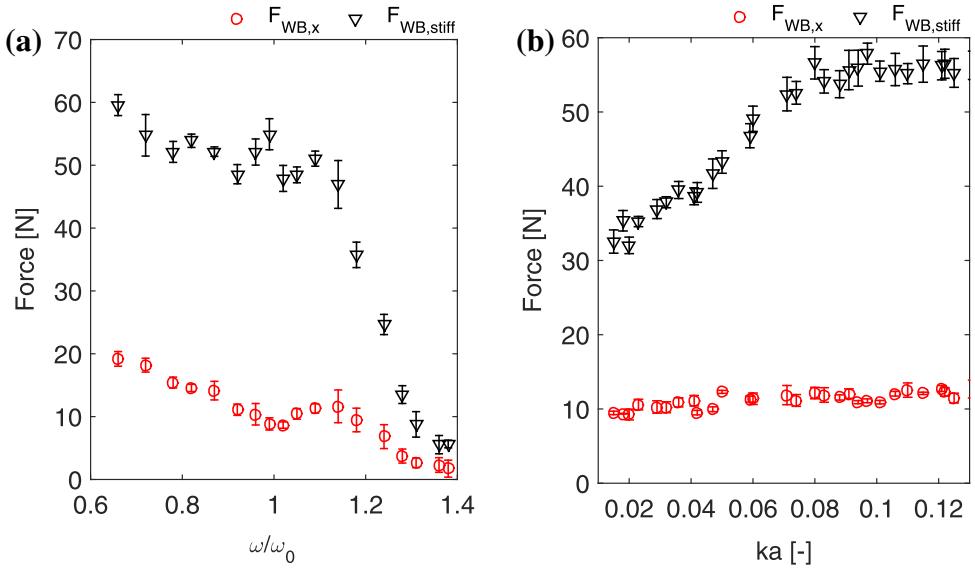

Fig. 7 **a** RMS values of measured forces versus frequency ratio for a constant ka. **b** RMS values of measured forces versus ka for a constant frequency ratio of $\frac{\omega}{\omega_0} = 1$. By using Eq. (2.7), the force reduction efficiency shown in Figs. 8 and 6, respectively, can be derived

value of η_r. The RMS values of absolute forces used to derive the force reduction efficiency as a function of the frequency ratio are shown in Fig. 7a. Each of the shown mean measurement points includes three separated measurements. The drop of the absolute forces on a stiff plunger with an increasing frequency ratio can be explained by the smaller incident wave height to keep the wave steepness ka in the mentioned range.

While keeping the frequency ratio $\frac{\omega}{\omega_0} = 1$, the effects of the wave steepness, ka, on the performance of the Wave Bridge were evaluated. Setting the frequency ratio to 1 guaranteed that we achieved the best performance for various wave steepnesses. Thus, the frequency of the wave maker was set to constant $f = 1.27$ Hz, while the wave maker's plunger draft was varied to achieve variable wave steepness conditions for the incident wave. Figure 8 shows the protection, force reduction, transmission, and reflection efficiencies of the Wave Bridge as a function of the wave steepness, ka. Again, each of the shown averaged measurement points include three actual measurements. The transmission and reflection efficiency data points were fitted to a fourth-order polynomial. A second-order polynomial fit was used for the protection and force reduction efficiencies. Additionally, a second abscissa was scaled to the plot, showing the accompanying a/h values.

The Wave Bridge transmission efficiency is relatively small at lower incident wave amplitudes in the range of $0.01 < ka < 0.05$. This is, in part, due to the initial dry friction that needs to be overcome before the Wave Bridge can transfer energy. In addition, the shape of the Wave Bridge is less effective at lower amplitude waves leading to a higher reflection of the incident wave energy, further resulting in a higher value of η_r. At higher ka values, however, the wave reflection decreases and the transferred energy increases,

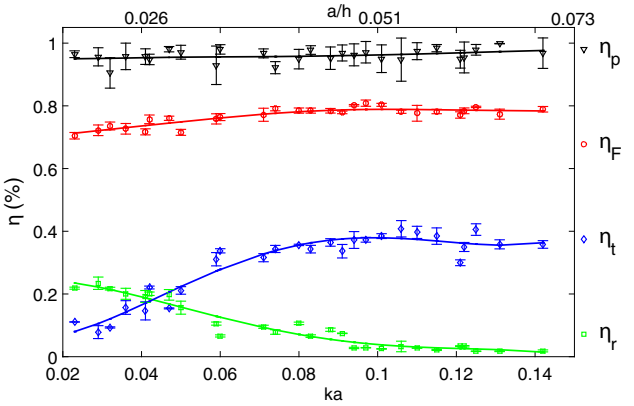

Fig. 8 The protection, force reduction, transmission and reflection efficiencies of the Wave Bridge for various incident wave steepnesses, ka. A reciprocal behavior of the transmission and reflection efficiencies is identified. Also, a higher wave transmission efficiency, η_t results in less horizontal net force applied to the Wave Bridge and a higher force reduction efficiency, η_F, ($h = 70$ cm, $f_{nat} = f_{wave} = 1.27$ Hz, $d_{plunger} = 46$ cm, vertical distance between plungers is 136 cm). Note that the protection efficiency, η_p, is the ratio of the wave energy in the protected area to the wave energy of the incident wave. Several parameters, including reflection of the waves from the Wave Bridge, may positively influence this efficiency. The transmission efficiency that is an overall measure of cumulative efficiencies of wave energy absorption and generation tops at ~40 %. Energy leakage from the side gaps are estimated by the ratio of the cumulative gaps on each side (~0.5 cm) to the overall width of the tank (45 cm), giving a side gap leakage of about ~ 2.2 %

reaching a maximum value of ~41 %. Contrary to the high influence of the wave steepness ka on η_t and η_r, the protection efficiency has slight gradient and stays above 90 %, independently of the transmission efficiency. The force reduction efficiency, which is derived from the absolute forces shown in Fig. 7b, consequently shows a high value above 70 %. Particularly, the absolute horizontal net forces on an operating

system as a function of the wave steepness ka show that the Wave Bridge concept can reach a high level of force protection for waves of different heights. Here, the increase of *ka* is directly proportional to the increase of the incoming wave height, since for these tests the frequency and thus k were kept constant. Therefore, the absolute force on a fixed plunger increases with higher ka values. Yet, the horizontal net force induced on the system in an operating mode stays nearly on an equal level. Waves in the protected zone are partly caused by leakage of incident wave energy underneath and through the side gaps between the plunger and the wave tank. Yet, by designing customized plungers, the side gaps were reduced to a minimum of 0.5 cm each. In the current investigation, the incident wave steepness, ka, is below 0.3 and thus the linear theory is applicable.

4 Wave leakage effects

In a real-life implementation, the wave absorber and wave emitter of the Wave Bridge will not reach the sea floor. Waves will partially leak underneath the plungers and decrease the protection efficiency of the Wave Bridge. Here, we present an estimation of percentage of energy leakage for a single plunger as a function of the ratio of the plunger height to the water depth i.e., d/h (Fig. 9). We would like to emphasize that the goal of this short section is not to present the solution to the wave maker or wave absorber problem, as such solutions are already provided by several prior works, e.g., Wang (1974), Wu (1988, 1991) for a plunger as a wave maker, and Hager et al. (2012), Count (1980), Evans (1976), Madhi et al. (2014) for a plunger as a wave absorber.

Consider the two-dimensional and linear problem of a wedge-shaped plunger of draft d in a water of depth h as shown in Fig. 9. Water is assumed to be incompressible and inviscid, and the velocity field is assumed to be irrotational, such that potential flow theory applies. The governing equation and linearized boundary conditions, respectively, at the air–water interface, seabed and on the plunger read

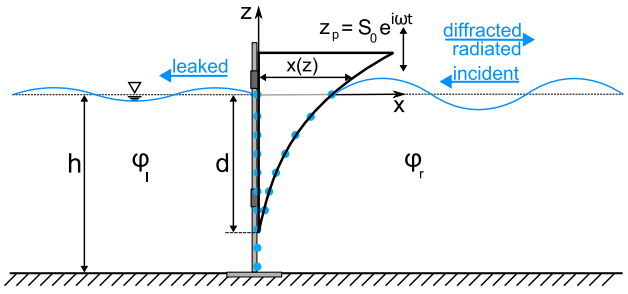

Fig. 9 Schematic diagram of the plunger-type wave energy converter in a finite water depth, h. The free surface water level is located at $z = 0$. The schematic is used for the numerical investigation of the leakage underneath the plunger

$$\nabla^2\varphi = 0, \quad -h < z < 0, \tag{4.1}$$

$$\varphi_{tt} + g\varphi_z = 0, \quad z = 0, \tag{4.2}$$

$$\varphi_z = 0, \quad z = -h, \tag{4.3}$$

$$\varphi_n = 0, \quad \text{on } S, \tag{4.4}$$

where φ is the velocity potential, S the boundary of the plunger, n normal to the surface S, g the gravitational acceleration, and subscripts of φ indicate partial derivatives. We denote the velocity potential on the right side of the plunger as φ_r, and on the left side as φ_l, i.e.,

$$\varphi = \begin{cases} \varphi_\mathrm{r}, & x > 0, \\ \varphi_\mathrm{l}, & x < 0. \end{cases} \tag{4.5}$$

To solve the radiation problem, we note that since the problem is linear and the plunger is undergoing periodic motion of frequency ω, the response of the waves will also be periodic with the same frequency ω. Each potential is represented by a general solution to the Laplace equation satisfying the bottom and surface boundary conditions. The potentials φ_r and φ_l differ only in the sign of their exponents which are to account for the radiation condition:

$$\varphi_\mathrm{r}(x,z,t) = \phi_\mathrm{r}(x,z)\mathrm{e}^{-i\omega t} = \left\{ A_0 \cos hk_0(z+h)\mathrm{e}^{ik_0 x} + \sum_{n=1}^{\infty} A_n k_n \cos k_n(z+h)\mathrm{e}^{-k_n x} \right\} \mathrm{e}^{-i\omega t}, \tag{4.6}$$

$$\varphi_\mathrm{l}(x,z,t) = \phi_\mathrm{l}(x,z)\mathrm{e}^{-i\omega t} = \left\{ B_0 \cos hk_0(z+h)\mathrm{e}^{-ik_0 x} + \sum_{n=1}^{\infty} B_n k_n \cos k_n(z+h)\mathrm{e}^{k_n x} \right\} \mathrm{e}^{-i\omega t}, \tag{4.7}$$

in which the frequency and wave numbers must satisfy the dispersion relations for the evanescent waves (index n) and the propagating wave (index 0):

$$\omega^2 = gk_0 \tanh k_0 h \quad \text{and} \quad \omega^2 = -gk_n \tan k_n h. \tag{4.8}$$

The plunger is located at $x = 0$ and its shape corresponds to the Wave Bridge plunger specified in (2.1). For a plunger with a draft of 0.55 m, the boundary conditions take the form

$$\frac{2.75}{\sqrt{(8.913x + 1.15)^2 - 1}}\phi_{r,x} + \phi_{r,z} = -i\omega S_0 \quad -d < z < 0, \quad x = \text{Eq. (2.1)} \tag{4.9}$$

$$\phi_{l,x} = 0 \quad -d < z < 0, \quad x = 0 \tag{4.10}$$

$$\phi_{r,x} = \phi_{l,x} \quad -h < z < -d \quad x = 0 \tag{4.11}$$

$$\phi_r = \phi_l \qquad -h < z < -d \quad x = 0, \tag{4.12}$$

where the first two equations satisfy the lateral no-flow boundary condition on the plunger surface and the last two equations state that the horizontal velocity and pressure below the plunger are the same on the left and right hand side.

To numerically solve this problem, we use a variation of the boundary collocation method (see e.g., Wu 1988). Let the entire water column be evenly divided into $M-1$ sections ($\delta h = h/(M-1)$). Thus, there will be M nodes for which boundary conditions have to be satisfied, each at the depth of $z_j = -j\ \delta h$, $j = 0, \ldots, M-1$. Assume out of these M nodes, q are along the side of the plunger. In other words, q nodes are above $z = -d$ or $(q-1)\delta h < d$. Obviously, the void area below the plunger has $p = M - q$ nodes. Each of the Eqs. (4.9) and (4.10) now lead to q equations, and each of Eqs. (4.11) and (4.12) lead to p equations, making the total number of equations $2(q+p)$. If n terms are chosen in the velocity potential expansion, the total number of unknowns in the series expansion (4.6) and (4.7) is $2(n+1)$. Therefore, $n+1 \leq M$, where equality gives a full rank equation and greater gives an overdetermined equation. To reduce errors in matrix operations, an overdetermined system is solved using least squares method.

The boundary collocation method is now implemented on an oscillating plunger to numerically estimate the amount of wave energy that leaks beneath the plungers of the Wave Bridge leading to the appearance of waves in the protected zone. The diffraction problem can be solved via BCM in a similar manner. In this case, the plunger is fixed and a linear wave impinges from the right on the plunger front. In numerical implementation, the stroke amplitude is set to zero ($S_0 = 0$) and an incident wave $\varphi_{\mathrm{r,in}} = C_0 \cos hk_0(z+h)\mathrm{e}^{-ik_0x}\mathrm{e}^{-i\omega t}$ is added to the potential of the wave on the right of the plunger φ_{r}. In both cases, the number of nodes and evanescent wave modes are chosen as $M = 200$ and $n = 8$, yielding convergence.

Figure 10a shows the leakage due to oscillation of the plunger (the radiation problem) as a function of d/h (i.e., the plunger depth normalized by the water depth) and λ/h (i.e., the wavelength scaled by the water depth). The vertical axis, $(a_{\mathrm{l}}/a_{\mathrm{r}})^2$ is the ratio of square of amplitude of radiated waves behind (i.e., leaked) and amplitude of waves in front of the plunger, hence providing a measure of the energy leakage. We call waves on the back side of the plunger *leaked* waves because an ideal wave maker is expected to send all the input energy to the right-going (i.e., desired) waves. Therefore any energy propagating in the opposite direction (leftward in Fig. 9) is leaked underneath the plunger. Figure 10a shows that radiated wave leakage is higher for longer waves and shorter plunger drafts.

We also present the leakage due to incident wave (the diffraction problem) in Fig. 10b. Here incident wave (amplitude a_{i}) is assumed to arrive from $x = +\infty$ and therefore a_{l} (amplitude on the left side of the plunger as shown in Fig. 9) is the amplitude of the leaked wave. Therefore, the quantity $(a_{\mathrm{l}}/a_{\mathrm{i}})^2$ shows the ratio of the leaked energy underneath the plunger to the energy of the incident wave. A trend similar to the radiation problem is observed. Specifically, longer waves leak more, and shorter plungers lead to higher leakages, as expected.

The numerical results for the wedge-shaped plunger imply that care must be taken in selecting the dimensions of the Wave Bridge plungers. The dimensions are dependent on the water depth, the dominant wavelength, and the target mag-

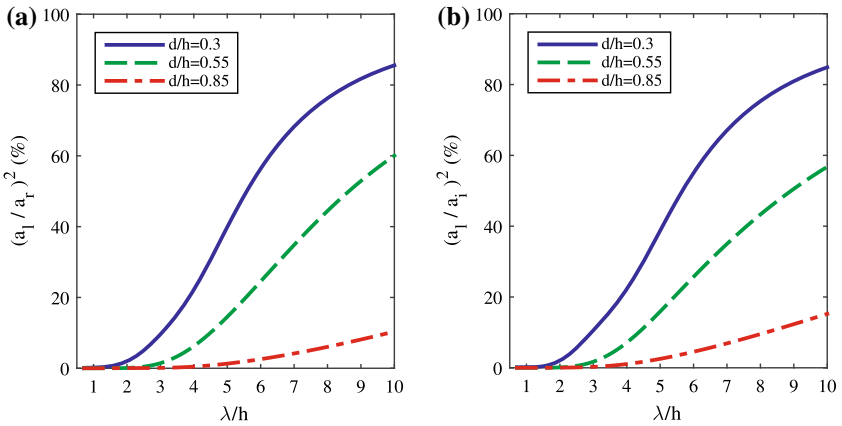

Fig. 10 **a** Leakage in the radiation problem, i.e., when the plunger oscillates vertically in the absence of an incident wave. The graph shows the ratio of the square of the amplitude of the wave on the *left* a_{l} (i.e., leaked) and the amplitude of the wave on the *right* of the plunger a_{r} as a function of λ/h, for various drafts of the wedge-shaped plunger. $M = 200$, $n = 8$, $h = 0.7$ m, $S_0 = 0.05$ m, **b** leakage in the diffraction problem, i.e., when an incident wave from the *right side* (cf. Fig. 9) arrives at a stationary plunger. The plot is the squared ratio of the amplitude on the *left side* of the stationary plunger (leaked amplitude) a_{l} to the amplitude of the incident wave a_{i}. Trends are similar to the radiation problem: longer waves and shorter plungers correspond to larger leaks. $M = 200$, $n = 8$, $h = 0.7$ m, $a_{\mathrm{i}} = 0.05$ m

nitude of the protection for the offshore structure. Higher protection requires a deeper draft of the plungers relative to the water depth. This is because the ratio of the left-going wave amplitude to the right-going wave amplitude approaches unity for most wave conditions when the draft of the body is small.

5 Conclusion

A new concept, called the Wave Bridge, for bypassing oceanic waves and horizontal momentum about ocean objects was experimentally and numerically investigated. The Wave Bridge is composed of a wave energy absorber and a wave maker that are connected via a linkage mechanism. The energy absorbed upstream of an ocean object by the wave energy absorber is mechanically transferred to the wave maker that is installed on the downstream side of the object. In other words, ocean wave energy is absorbed on the upstream side of the ocean object and spent to generate similar waves downstream of that object. Hence the structure is nearly *cloaked* against the waves, since waves are bypassed around the ocean object using the Wave Bridge. Furthermore, the horizontal forces on the wave energy absorber and wave maker are the same, but opposite. As a result, the net horizontal force on the structure protected by the Wave Bridge is relatively low. We have shown via laboratory experiments that a wave protection efficiency of up to 97 % and a horizontal force protection efficiency of up to 80 % is achievable. The numerical results show that the Wave Bridge protection depends on the plunger draft, the water depth, and the wave length. For a deployment of the Wave Bridge in a real sea environment, further studies are needed to investigate the performance of the device under nonlinear and broadband waves conditions as well as the effects of scaleup.

The Wave Bridge idea can be extended for shielding against omnidirectional waves by, say, attaching a number of finite-width bridges at different angles about the structure, or, by a cylinder-like Wave Bridge that fully surrounds the offshore structure.

Acknowledgments We would like to thank Marcus Lehman and Ryan Elandt for their help. Support from the American Buearu of Shipping is gratefully acknowledged.

References

Count B (1980) Power from sea waves: based on the proceedings of a conference on power from sea waves. In: The Institute of Mathematics and its applications series. Academic Press, New York

Dong GH, Zheng YN, Li YN, Teng B, Guan CT, Lin DF (2008) Experiments on wave transmission coefficients of floating breakwaters. Ocean Eng 35(8–9):931–938. doi:10.1016/j.oceaneng.2008.01.010

Ellix D, Arumugam K (1984) An experimental study of waves generated by an oscillating wedge. J Hydraul Res 22(5):299–313. doi:10.1080/00221688409499367

Evans DV (1976) A theory for wave-power absorption by oscillating bodies. J Fluid Mech 77(1):1–25

Goda Y, Suzuki T (1976) Estimation of incident and reflected waves in random wave experiments. doi:10.9753/icce.v15

Hager R, Fernandez N, Teng MH (2012) Experimental study seeking optimal geometry of a heaving body for improved power absorption efficiency. In: Proceedings of the 22nd international offshore and polar engineering conference (ISOPE-2012), Greece, June 2012

Hales LZ (1981) Floating breakwaters: state-of-the-art literature review. Fort Belvoir, Va.: U.S. Army, Corps of Engineers, Coastal Engineering Research Center; Springfield, Va.: National Technical Information Service, distributor (1981)

He F, Huang Z, Wing-Keung Law A (2012) Hydrodynamic performance of a rectangular floating breakwater with and without pneumatic chambers: an experimental study. Ocean Eng 51:16–27. doi:10.1016/j.oceaneng.2012.05.008

Henderson DM, Patterson MS, Segur H, Pritchard WG (2006) On the laboratory generation of two-dimensional, progressive, surface waves of nearly permanent form on deep water. J Fluid Mech 559:413–427. doi:10.1017/S0022112006000103

Madhi F, Sinclair ME, Yeung RW (2014) The "Berkeley wedge": an asymmetrical energy-capturing floating breakwater of high performance. Mar Syst Ocean Technol 9(1):5–16

Patel MH, Ionnaou PA (1980) Comparative performance study of paddle- and wedge-type wave generators. J Hydronaut 14(1):3–7

Wang S (1974) Plunger-type wavemakers: theory and experiment. J Hydraul Res 12(3):357–388

Wu YC (1988) Plunger-type wavemaker theory. J Hydraul Res 26:483–491. doi:10.1080/00221688809499206

Wu YC (1991) Waves generated by a plunger-type wavemaker. J Hydraul Res 29(6):851–860. doi:10.1080/00221689109498963